Journal of Power Sources 191 (2009) 371–376

Contents lists available at ScienceDirect

Journal of Power Sources

journal homepage: www.elsevier.com/locate/jpowsour

High performance metal-supported solid oxide fuel cells fabricated by thermal spray

Rob Hui[a,*], Jörg Oberste Berghaus[b,1], Cyrille Decès-Petit[a], Wei Qu[a], Sing Yick[a], Jean-Gabriel Legoux[b], Christian Moreau[b]

[a] National Research Council of Canada – Institute for Fuel Cell Innovation, 4250 Wesbrook Mall, Vancouver, BC, V6T 1W5 Canada
[b] National Research Council of Canada – Industrial Materials Institute, 75 de Mortagne Boulevard, Boucherville, Quebec, J4B 6Y4 Canada

ARTICLE INFO

Article history:
Received 16 January 2009
Received in revised form 19 February 2009
Accepted 20 February 2009
Available online 6 March 2009

Keywords:
Solid oxide fuel cells (SOFCs)
Metal-supported
Low temperature
Thermal plasma spray
High performance

ABSTRACT

Metal-supported solid oxide fuel cells (SOFCs) have been fabricated and characterized in this work. The cells consist of porous NiO–SDC as anode, thin SDC as electrolyte, and SSCo as cathode on porous stainless steel substrate. The anode and electrolyte layers were consecutively deposited onto porous metal substrate by thermal spray, using standard industrial thermal spray equipment, operated in an open-air atmosphere. The cathode materials were applied to the as-sprayed half-cells by screen-printing and heat-treated at 800 °C for 2 h. The cell components and performance were examined by scanning electron microscopy (SEM), X-ray diffraction, leakage test, ac impedance and electrochemical polarization at temperatures between 500 and 700 °C. The half-inch button cells exhibit a maximum power density in excess of 0.50 W cm^{-2} at 600 °C and 0.92 W cm^{-2} at 700 °C operated with humidified hydrogen fuel, respectively. The half-inch button cell was run at 0.5 A cm^{-2} at 603 °C for 100 h. The cell voltage decreased from 0.701 to 0.698 V, giving a cell degradation rate of 4.3% kh^{-1}. Impedance analysis indicated that the cell degradation included 4.5% contribution from ohmic loss and 1.4% contribution from electrode polarization. The 5 cm × 5 cm cells were also fabricated under the same conditions and showed a maximum power density of 0.26 W cm^{-2} at 600 °C and 0.56 W cm^{-2} at 700 °C with dry hydrogen as fuel, respectively. The impedance analysis showed that the ohmic resistance of the cells was the major polarization loss for all the cells, while both ohmic and electrode polarizations were significantly increased when the operating temperature decreased from 700 to 500 °C. This work demonstrated the feasibility for the fabrication of metal-supported SOFCs with relatively high performance using industrially available deposition techniques. Further optimization of the metal support, electrode materials and microstructure, and deposition process is ongoing.

1. Introduction

Metal-supported solid oxide fuel cells (SOFCs) have been recognized as a promising alternative to conventional cermet- or ceramic-supported SOFCs. The metal-supported, such as stainless steel supported SOFCs exhibit high mechanical strength, good ductility, and matching thermal expansion coefficient with zirconia- and ceria-based electrolytes. Structural limitations arise not only from the thermal stress at rapid start-up and during temperature fluctuations; but also from the mechanical stress from assembly compaction and vibrations. Therefore, metal-supported SOFCs fulfil the requirements of structural robustness and thermal shock resistance with low internal temperature and stress gradients. Stainless steels are available commercially in a wide range of compositions and microstructures. The unit price of steel is at least one order of magnitude lower than the ceramic components such as NiO and YSZ. Thus, the total material cost can be reduced significantly. Metallic substrates can be easily fabricated into desired shapes, such as planar, circular tubular, and flat tubular by traditional machining at low cost. The use of metallic substrates allows the use of conventional metal joining and forming techniques, and could significantly reduce the manufacturing costs of SOFC stacks. In comparison, glass–ceramic sealants used in electrolyte- and electrode-supported SOFCs need to provide adherence, electrical insulation, chemical stability and compatibility, as well as protection against mechanical degradation from stress during operation. The structural instability resulting from start-up and thermal cycling is usually regarded as one of the main causes of cell breakage and stack failure [1]. Due to these potential merits of metal-supported SOFCs, significant technical progresses have been

* Corresponding author.
E-mail address: Rob.hui@nrc-cnrc.gc.ca (R. Hui).
[1] Current address: Bekaert Advanced Coatings NV, E3-Laan 75-79, Deinze, 9800, Belgium.

0378-7753/$ – see front matter.
doi:10.1016/j.jpowsour.2009.02.067

achieved at research groups world wide including the National Research Council of Canada [2–5], the Aerospace Research Centre and Space Agency (DLR) [6,7], Ceres Power and Imperial College [8,9], Research Centre Jülich (FZJ) [10], Lawrence Berkeley National Laboratory (LBNL) [11–13], Nippon Coating Industry Co. and University of Hyogo in Japan [14,15].

One of the major challenges for the development of metal-supported SOFCs is the cell fabrication process without oxidizing the metallic substrate and with potentially low cost for commercialization. Plasma thermal spray is a well established and proven technology, which is already in widespread industrial use for a variety of applications due to the low cost and simplicity of the processes [16,17]. This deposition technique has the potential to fabricate SOFCs at temperatures below 700 °C with no further heat-treatments as required for the sintering of ceramic components [5,18–29]. Particularly, the density of the thermal spray coatings has been improved by a combination of high-velocity oxy-fuel (HVOF) and suspension feedstock. Killinger et al. [30] and Oberste Berghaus et al. [31] have reported the feasibility to deposit ceramic oxides using HVOF and suspension feedstock with different fuels. The advantages of suspension feedstock over the conventional powder feedstock for SOFC fabrication have also been demonstrated [26]. Employing suspension feedstock, metal-supported SOFCs have been produced by consequent depositions through air plasma thermal spray and HVOF in this work. The electrochemical performance of the cells and feasibility for scale-up were also studied.

2. Experimental

Porous Hastelloy X plates (Mott Corp., Farmington, CT, USA) were used as metallic substrates for the SOFC fabrication. The substrate is 1.25 mm thick with a 27.5% porosity determined by Archimedes's method. The substrates were cut into 12.7 mm diameter discs or 5 cm × 5 cm squares and were cleaned in acetone before anode deposition.

Nano-sized $Ce_{0.8}Sm_{0.2}O_{2-\delta}$ (SDC) powders (80–220 $m^2\,g^{-1}$, nGimat) were used as electrolyte materials and their suspension was sprayed on the top of the anode layer using an HVOF DJ-2700 hybrid gun (Sulzer-Metco) with propylene fuel (C_3H_6). The suspension was delivered by a prototype Nanofeed Liquid Powder Feeder (Model 640, Northwest Mettech) with a computer-controlled process. NiO–SDC (50:50, wt%) anode materials was mixed from NiO powders (d_{50}—14.4 μm, 0.21 $m^2\,g^{-1}$, Inco) and SDC powders (8.9 $m^2\,g^{-1}$, Nextech Materials). The anode layer was deposited on the Hastelloy X substrates by suspension plasma spray with an axial feed injection torch (Axial III, Northwest Mettech). All the suspensions of ceramic powders were made in ethanol with ethylene glycol and polyethylenimine (MWT 25,000 Alfa Aesar) as additives. Surface temperature of the substrate, as monitored by a pyrometer, was controlled to below 700 °C during deposition. The detailed conditions for the cell fabrication were discussed in a separate publication [5].

After the deposition of anode and electrolyte, the half-cells were subjected to a helium leak test at 1psi differential pressure. A cathode paste was made by ball-milling a mixture of 75 wt% $Sm_{0.5}Sr_{0.5}CoO_3$ (SSCo) powder, 25 wt% SDC powder, an appropriate amount of isopropyl alcohol and wax in actane. The composite cathode paste was screen-printed on the half-cell and fired *in situ* at 800 °C for 2 h, resulting in a thickness of around 45 μm. Pt meshes were used as current collectors in both the anode and the cathode sides of the button cell. Corrugated stainless steel 430 and nickel foam was used as current collectors on the cathode and the anode side for the square cells, respectively. The effective area is 0.34 cm^2 for the button cells and 9 cm^2 for the 5 cm × 5 cm cells. The cells were maintained at 650 °C for 5 h while gradually introducing hydrogen to reduce NiO to Ni in the anode. The hydrogen was introduced to the anode with an increased concentration of 20%, 40%, 60%, 80%, and 100% balanced with nitrogen with a flow rate of 100 sccm. The electrochemical polarization curves were measured from 500 to 700 °C in 50 °C intervals. The electrochemical performance and the ac impedance measurements were performed twice with hydrogen saturated with water at 21 °C as fuel and air as oxidant at each temperature. The flow rates of hydrogen and air used for the impedance measurements were 100 sccm, respectively. The polarization characteristics were measured using a Solartron 1480A Multistat with a slew rate of 4 mV s^{-1} in the potential range from open circuit voltage (OCV) to 0.3 V. The ac impedance spectra were obtained in the frequency range of 100 kHz to 0.1 Hz under OCV conditions with 50 mV AC amplitude using a Solartron 1260 frequency response analyzer (FRA) connected to the Solartron 1480A Multistat. A porous alumina felt was used as the sealant on the anode side. Details of the testing setup are published in our previous work [2,4]. Phase analysis was carried out by XRD using a Brucker D8-Discovery diffractometer (Brucker AXS Inc.) with Cu Kα radiation at 0.01° s^{-1}. The cross-sectional microstructures of the cells were examined with a Hitachi S-3500N scanning electron microscope (SEM).

3. Results and discussion

3.1. Half-inch button cells

The helium leak rates of the half-cells were measured at 1 psi (6.9 kPa) differential pressure for a period of 5 min. No leak of helium was detected for the half-inch button cell with an electrolyte fabricated by HVOF. Compared to the cells with electrolyte fabricated by atmospheric plasma spray (APS) the leaking rates range from 0.07 to 0.11 sccm. The microstructures of the cell components were examined after the polarization test. The cross-sectional SEM image for the cell with an electrolyte fabricated by HVOF is shown in Fig. 1. In general, the different layers were bonded very well, except delaminations were observed on some spots between the cathode and the electrolyte layers. The typical lamellar structure for thermal sprayed coatings can be identified on the anode layer but not on the electrolyte layer. However, the lamellar structure is much finer than the conventional plasma spray using powder feedstock with a particle size around 40 μm. The microstructure of the cathode layer was not uniform and some large particles were observed. The EDX results indicated that these large particles in the cathode were SDC most likely formed through agglomeration of small SDC particles

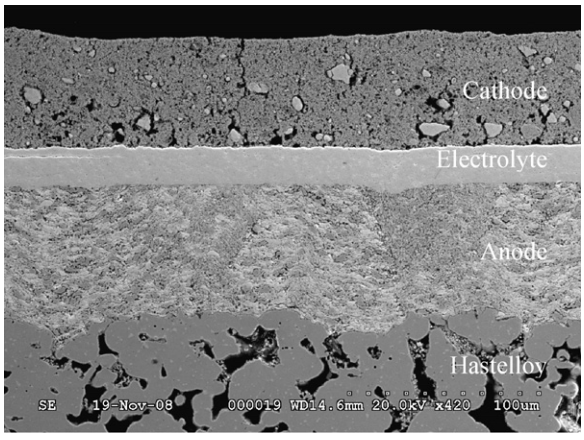

Fig. 1. SEM image of the cross-section of the half-inch button cell after electrochemical and thermal cycling tests.

distributed unevenly in the cathode composite. Therefore, the dispersion of the SDC powder in the composite cathode needs to be improved in the future. The observed partial delamination between cathode and electrolyte could be due to the thermal mismatch and the low temperature processing. The cathode was screen-printed and fired at 800 °C for 2 h only, which might lead to a change in microstructure during the cell operation and poor bonding with the electrolyte. This issue has been observed in our previous work for cells fabricated by suspension plasma spray (SPS) [4]. The cathode may also be deposited on the top of electrolyte layer by SPS to improve the adhesion in the future.

Compared with the electrolyte layer built by SPS [3,4], the electrolyte layer fabricated by HVOF is much denser and free of cracks or pinholes. The density of the electrolyte layer is greater than 98% estimated by the SEM image analysis. XRD analysis revealed that the electrolyte layer was crystallized SDC with a grain size of approximately 37 nm. Plasma spray offers a flame temperature above 8000 °C in a reducing atmosphere, which may lead to some vaporization and decomposition of CeO_2 to Ce_2O_3 [20,32]. This could be more serious for the small particle in suspension as feedstock. In addition, these effects may result in poor quality of the SDC electrolyte layer in terms of deposition efficiency, mechanical integrity, and electrochemical performance due to increased electronic conduction from Ce^{4+} to Ce^{3+}. HVOF provides a much lower flame temperature (2600–3200 °C) but higher velocity of the sprayed particles [20]. The flame temperature in HVOF is lower than that in thermal plasma spray, but the temperature is still higher than the melting temperature of SDC (~2730 °C). The high velocity of the flame would be helpful for the small particles in suspension to increase their momentum for denser coatings. The oxidizing atmosphere in HVOF also favours the stabilization of Ce^{4+} in SDC. The flame temperatures in HVOF was adjusted according to the torch design, the fuel and fuel-to-oxygen ratio, the particle size and feed rate of the SDC feedstock, and the deposition distance in this work. Tensile stresses that generally arise due to the material shrinkage during solidification of the molten droplets, often lead to transverse cracks in thermal plasma spray coatings [21]. The as-sprayed materials may also have a phase transformation from amorphous to crystalline during post-heat-treatment or application at elevated temperatures, which may lead to volume change and cracks as well [21]. Using HVOF, these stresses may be partially compensated by the plastic deformation of unmelted or partially molten and ductile ceramic particles impacting at high velocity [26]. Under the spray conditions in this work, a substantial portion of the particles are likely not fully molten and their impact at nearly 900 m s^{-1} may affect the intrinsic stresses by introducing a compressive component. Therefore, in HVOF suspension spraying, the thermal stresses and local overheating, a severe limitation for atmospheric pressure thermal spraying of SOFC electrolytes [23], can be managed. Furthermore, the top surface of the electrolyte is relatively smooth without the humps and defects often seen in SPS [31]. The impacting colder particles may remove loosely attached material during deposition and lead to this low surface roughness.

The electrochemical polarization and the impedance of the whole cells were measured after the anodes were reduced from 500 to 700 °C. The OCV is 0.97 V at 500 °C and 0.82 V at 700 °C as shown in Fig. 2. These OCV values are close to those of SDC electrolyte fabricated by screen-printing process [33]. Doped-ceria is a purely oxide ionic conductor under oxidizing atmosphere. It is well known that doped-ceria become a mixed ionic and electronic conductor due to the partial reduction of Ce^{4+} into Ce^{3+} under reducing conditions at elevated temperatures. The ionic transport numbers of ceria-based electrolytes are a function of oxygen partial pressure and temperature that determined the reduction level of Ce^{4+} to Ce^{3+} [34]. Therefore, the OCV of a cell based on doped-ceria electrolyte depends on several parameters including oxygen partial

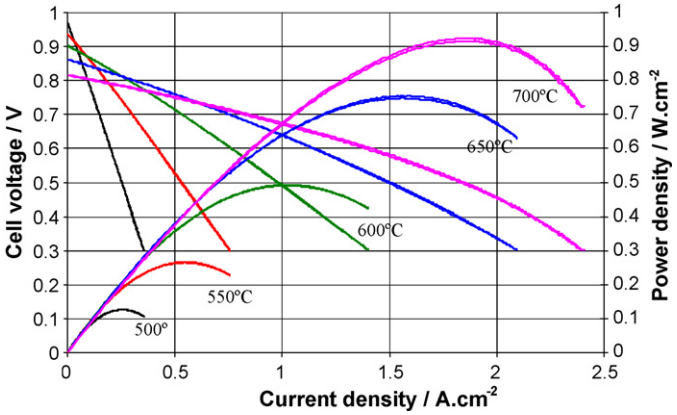

Fig. 2. Electrochemical performance of the half-inch button cell (fuel: 97% H_2 with 3% H_2O, oxidant: air).

pressure, temperature, and thickness related to the reduction gradient across the electrolyte [35,36]. The theoretical OCV could not be calculated directly using the standard Nernst equation. An effort has been done to calculate the theoretical OCV [37,38]. However, a good agreement between the calculated and the experimental data has not been achieved yet. It has to be noticed that the ionic radius of Ce^{3+} (0.115 nm) is larger than that of Ce^{4+} (0.101 nm). The reduction of Ce^{4+} to Ce^{3+} not only leads to an increased electronic conduction, but also induces a stress in the structure [39]. The induced stress may result in micro-cracks in the electrolyte, which could also affect the OCV during the cell operation. This may be a more serious issue for cells with thin film ceria-based electrolyte. In order to use doped-ceria as an electrolyte without loss of fuel utilization efficiency, the electronic conduction at low oxygen partial pressure has to be suppressed [40–42]. Through a mathematical model, Leah et al., reported that the electronic leaking current depends on the external current density and operation temperatures [9]. The efficiency loss due to the electronic conduction may not be significant when the operation temperature is low and the external current density is high. Without the concern of the fuel utilization, the electrochemical performance of the cells based on SDC electrolyte and metallic support is very promising as shown in Fig. 2. The maximum power was 0.92 W cm^{-2} at 700 °C, which is compatible with the cermet-supported cells. This result is a significant progress compared with our previous results as well as other published results for metal-supported SOFCs [4,20,25]. The maximum power density decreased to 0.50 W cm^{-2} at 600 °C, indicating a need for high performance electrode materials and highly conducting electrolyte materials at low temperatures.

The cell impedances were measured at different temperatures and were plotted in Fig. 3. The ohmic loss was much higher than that of the electrode polarization loss at temperatures between

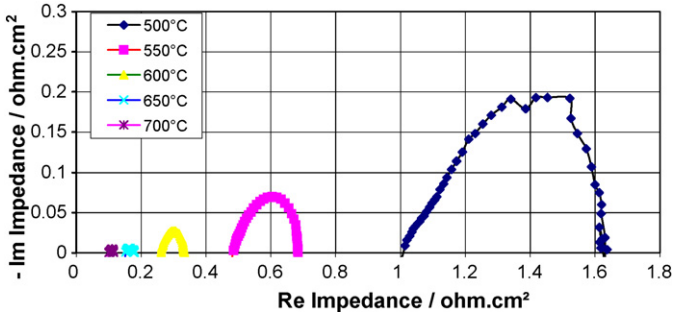

Fig. 3. Impedance change of the button cell with temperature.

500 and 700 °C. Above 600 °C, the contribution of the polarization resistance to the total resistance is almost negligible. This suggests that catalytic activity of the electrodes is not a limiting factor above 600 °C. However, at lower temperatures, both ohmic and polarization resistance increased significantly. Ohmic resistance is generally attributed to restricted ion conductivity through the electrolyte for cermet-supported SOFCs [33]. Hui et al. have studied the ionic conductivities between plasma sprayed $La_{0.8}Sr_{0.2}Ga_{0.8}Mg_{0.2}O_{3-\delta}$ (LSGM) and sintered ones [21]. No significant difference was observed for the electrical conductivities for the LSGM electrolytes made by the two different processes. However, since the melting temperature of SDC is much higher than that of LSGM, the density and microstructure of LSGM and SDC deposited by thermal spray may be also different. Further characterization for HVOF sprayed SDC electrolyte may be needed to understand the ionic conductivity compared to the sintered bodies. On the other hand, an imperfect contact between the electrolyte and the electrodes may also contribute to both polarization and ohmic resistance. Indeed, the interfaces proved to be of limited quality. Thermal cycling tests at a heating rate of 60 °C min^{-1}, i.e., heating the cell from 25 to 600 °C in 10 min for multiple times, were conducted. The polarization loss and the ohmic loss were plotted versus number of thermal cycles in Fig. 4. Post-examination revealed some delamination on the cathode–electrolyte interface that might contribute to the significant increase in overall cell resistance. The OCV remained stable throughout the tests. As seen in Fig. 2 the electrolyte appears unaltered, which is consistent with the constant OCV. The potential micro-cracks chemically induced through reduction of Ce^{4+} to Ce^{3+} may lead to increased ohmic resistance as well.

The voltage variation of the metal-supported SOFC under a constant current of 0.5 A cm^{-2} at 603 °C is given in Fig. 5. Considering that the highest voltage was 0.701 V at the beginning and the lowest value was 0.698 V after 100 h, the degradation rate is 4.3% kh^{-1} over a period of 100 h. The change of cell impedance was recorded before and after the stability test. The ohmic resistance increased 4.5% and the electrode polarization loss increased 1.4% during the 100 h. The ohmic loss is almost three times higher than that of electrode polarization. There are many factors that could contribute to the cell degradation, such as the oxidation of metallic substrate under humidified hydrogen atmosphere, sintering and microstructure change of anode and cathode, the delamination of cathode due to the low temperature *in situ* firing, and the change of SDC microstructure due to the reduction expansion. All these parameters need to be evaluated separately in the future to further improve the performance and the stability for a longer operation period.

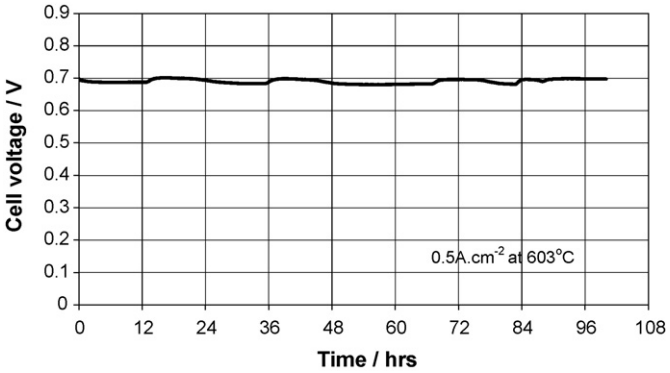

Fig. 5. Stability of electrochemical performance of the button cell measured at a current density of 0.5 A cm^{-2} at 603 °C.

3.2. 5 cm × 5 cm square cells

Metal-supported cells with a size of 5 cm × 5 cm were also prepared under the same conditions as the button cells in order to assess the feasibility for scale-up of cell fabrication. In spite of the relatively high surface temperature (440 °C) and the localized heating by the impinging spray jet, no distortion was observed on the substrate during or after thermal spray. Deposition at relatively large standoff distances (~13 cm) was made possible by the ongoing heating of the particles far outside the HVOF gun as they approach the substrate. This stands in contrast to SPS, where the small particles cool rapidly after exiting the torch and the substrate must consequently be placed in close proximity to the plasma [5]. In this way, the thermal stresses and local overheating is managed in HVOF suspension spraying, which is a severe limitation for APS of electrolytes for SOFCs [23]. No visible defects on the electrolyte surface could be detected optically. The helium leak rates of the half-cells were between 0.020 and 0.028 sccm at 1psi differential pressure, depending on the cells. The polarization *I–V* curves were plotted in Fig. 6 from 500 to 700 °C. The OCVs at different temperatures were close to the values of half-inch button cells as discussed above, indicating the quality of the electrolyte layer was not affected by the scale-up. The impedance measurements for the whole cell at different temperatures were summarized in Fig. 7. Similar to the button cells, the ohmic loss was much higher than that of the electrode polarization loss at temperatures between 500 and 700 °C.

The stability of the voltage for the 5 cm × 5 cm cells was also studied under a constant current of 0.226 A cm^{-2} at 662 °C as shown in Fig. 8. The degradation rate is 12.4% kh^{-1} over a period of 100 h, which is almost three times higher than that of the button cell. The

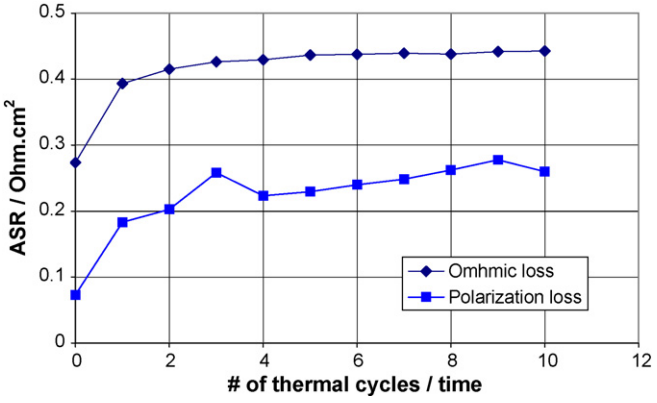

Fig. 4. Change of polarization loss and ohmic loss of the button cell with thermal cycling.

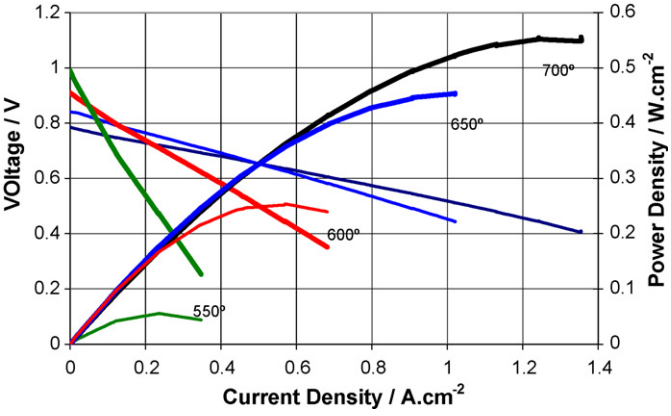

Fig. 6. Electrochemical performance of the 5 cm × 5 cm cell (fuel: 100% H_2, oxidant: air).

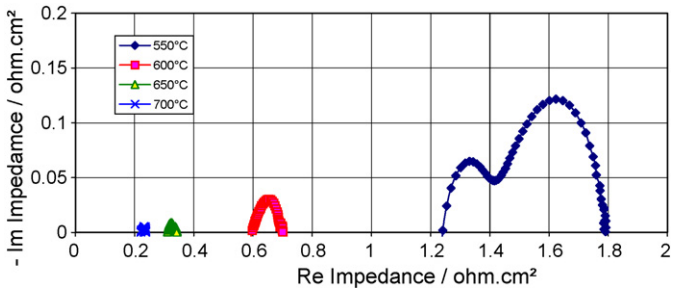

Fig. 7. Impedance variation of the 5 cm × 5 cm cell as a function of temperature.

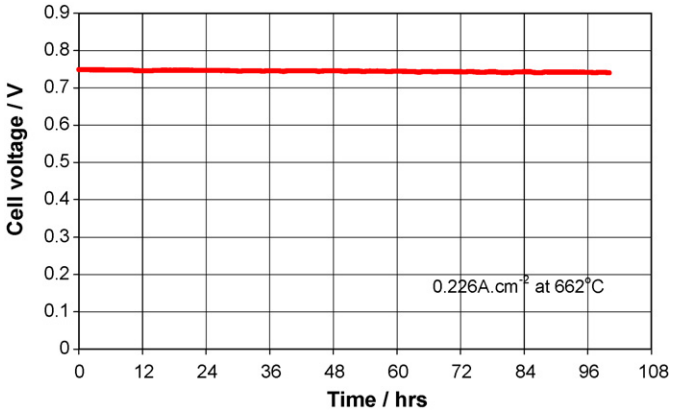

Fig. 8. Stability of electrochemical performance of the 5 cm × 5 cm cell.

impedance analysis before and after the stability evaluation indicated that the ohmic resistance increased 15% and the electrode polarization loss increased 5% during the 100 h. Again, the ohmic loss is three times higher than that of the electrode polarization, which is similar to the case of the button cell. Apart from the possible factors for the ohmic and polarization loss as discussed on the button cell, the employment of corrugated stainless steel as current collector for the cathode may have also contributed to the loss of performance. The chemical reactions and the Cr-poisoning at the cathode have been well reported in the literature [43–47]. A protective coating to avoid the Cr-poisoning on the stainless steel current collector or Cr-resistant cathode materials are needed to improve the cell stability against the performance degradation.

4. Conclusions

The combination of suspension thermal plasma spray for the porous anode layer and the suspension HVOF spray for the dense electrolyte layer have been demonstrated to be a successful approach for the fabrication of metal-supported SOFCs. Without further post-sintering of the ceramic components, the maximum power density operated with humidified hydrogen fuel for a half-inch button cell was 0.50 W cm^{-2} at 600 °C and 0.92 W cm^{-2} at 700 °C, respectively. The degradation rate for the cell was 4.3% kh^{-1} for a period of 100 h at 600 °C. The 5 cm × 5 cm cells were also fabricated under the same conditions as the half-inch button cells. The maximum power density with humidified hydrogen as fuel was 0.26 W cm^{-2} at 600 °C and 0.56 W cm^{-2} at 700 °C, respectively. The easy scale-up of the process makes the techniques promising for the potential commercialization of metal-supported SOFCs. The impedance analysis for the cells indicated that the ohmic polarization was the major loss for the electrochemical performance and the degradation. The cell performance could be potentially further improved at low temperatures by prevention of metallic substrate oxidation and Cr-poisoning on cathode, stabilization of the cathode microstructure and adhesion to the electrolyte, and employment of high performance cathode and electrolyte materials in the future. Further comparison studies of ionic conductivity for the HVOF sprayed SDC and the sintered one may also be needed in order to understand the observed high ohmic loss in this work.

Acknowledgement

Thanks to the National Fuel Cell and Hydrogen Program of the National Research Council of Canada for the financial support of this work.

References

[1] S.C. Singhal, Solid State Ionics 152–153 (2002) 405–410.
[2] S. Hui, D. Yang, Z. Wang, S. Yick, C. Decès-Petit, W. Qu, A. Tuck, R. Maric, D. Ghosh, J. Power Sources 167 (2007) 336–339.
[3] Q. Huang, J.O. Berghaus, D. Yang, S. Yick, Z. Wang, B. Wang, R. Hui, J. Power Sources 177 (2008) 339–347.
[4] Z. Wang, J.O. Berghaus, S. Yick, C. Decès-Petit, W. Qu, R. Hui, R. Maric, D. Ghosh, J. Power Sources 176 (2008) 90–95.
[5] J.O. Berghaus, J.-G. Legoux, C. Moreau, R. Hui, C. Decès-Petit, W. Qu, S. Yick, Z. Wang, R. Maric, D. Ghosh, J. Therm. Spray Technol. 17 (5) (2008) 700–706.
[6] G. Schiller, T. Franco, M. Lang, P. Metzger, A.O. Störmer, Electrochem. Soc. Proc. 07 (2005) 66–75.
[7] G. Schiller, T. Franco, R. Henne, M. Lang, R. Ruckdäschel, Electrochem. Soc. Proc. 16 (2001) 885–894.
[8] P. Attryde, A. Baker, S. Baron, A. Blake, N.P. Brandon, d. Corcoran, D. Cumming, A. Duckett, K. El-Koury, D. Haigh, M. Harrington, C. Kidd, R. Leah, G. Lewis, C. Matthews, N. Maynard, T. McColm, A. Selcuk, M. Schmidt, R. Trezona, L. Verdugo, Electrochem. Soc. Proc. 07 (2005) 113–122.
[9] R.T. Leah, N.P. Brandon, P. Aguiar, J. Power Sources 145 (2005) 336–352.
[10] D. Stöver, D. Hathiramani, R. Vaßen, R.J. Damani, Surf. Coat. Technol. 201 (2006) 2002–2005.
[11] S.J. Visco, C.P. Jacobson, I. Villareal, A. Leming, Y. Matus, L.C.D. Jonghe, Electrochem. Soc. Proc. 07 (2003) 1040–1050.
[12] I. Villareal, C.P. Jacobson, A. Leming, Y. Matus, S.J. Visco, L.C.D. Jonghe, Electrochem. Solid-State Lett. 6 (9) (2003) A178–A179.
[13] Y.B. Matus, L.C.D. Jonghe, C.P. Jacobson, S.J. Visco, Solid State Ionics 176 (2005) 443–449.
[14] A. Momma, Y. Kaga, T. Okuo, K. Fujii, K. Hohjyo, M. Kanazawa, Bull. Electrotech. Lab. 63 (3) (1999) 1–11.
[15] A. Mineshige, K. Fukushima, S. Okada, T. Kikuchi, M. Kobune, T. Yazawa, K. Kikuchi, M. Inaba, Z. Ogumi, Electrochem. Solid-State Lett. 9 (9) (2006) A427–A429.
[16] O. Kesler, M. Finot, S. Suresh, S. Sampath, Acta Mater. 45 (1997) 3123–3134.
[17] O. Kesler, J. Matejicek, S. Sampath, S. Suresh, T. Gnaeupel-Herold, P.C. Brand, H.J. Prask, Mater. Sci. Eng. A 257 (1998) 215–224.
[18] S. Hui, J. Broadhead, T.D. Xiao, International patent, WO 03/075383 A2.
[19] J. O. Berghaus, R. Hui, US patent pending.
[20] R. Hui, Z. Wang, O. Kesler, R. Maric, D. Ghosh, J. Power Sources 170 (2) (2007) 308–323.
[21] S. (Rob) Hui, H. Zhang, J. Dai, X. Ma, T.D. Xiao, D.E. Reisner, Eighth International Symposium on Solid Oxide Fuel Cells (SOFC-VIII), Paris, France, April 27–May 2, 2003.
[22] S. Hui, H. Zhang, X. Ma, J. Roth, T.D. Xiao, D.E. Reisner, Fuel Cell 2003—The Third Annual BCC Conference: Connections to Commercialism, Stamford, CT, USA March 31–April 1, 2003.
[23] S. (Rob) Hui, J. Dai, J. Roth, D. Xiao, MRS Fall Meeting, Boston, 2003.
[24] X.Q. Ma, D. Xiao, H. Zhang, J. Dai, R. Hui, D.E. Reisner, International Thermal Spray Conference (ITSC), FL, May 1, 2003.
[25] R. Henne, J. Therm. Spray Technol. 16 (3) (2007) 381–402.
[26] R. Gadow, A. Killinger, A. Candel Ruiz, H. Weckmann, A. Öllinger, O. S Patz, Proceedings of the 2007 International Thermal Spray Conference Global Coatings Solutions, May 14–16 (Beijing, China), ASM International, 2007, pp. 1053–1058.
[27] D. Stöver, R. Dag Hathiramani, R.J. Vaβen, Damani, Surf. Coat. Technol. 201 (2006) 2002–2005.
[28] P. Fauchais, R. Etchart-Salas, C. Delbos, M. Tognonvi, V. Rat, J.F. Couder, T. Chartier, J. Phys. D.: Appl. Phys. 40 (2007) 2394–2406.
[29] J. Oberste Berghaus, J.-G. Legoux, C. Moreau, R. Hui, D. Ghosh, Mater. Sci. Forum, Trans. Tech. Publisher, Switzerland, 539–543 (2007) 1332–1337.
[30] A. Killinger, M. Kuhn, R. Gadow, Surf. Coat. Technol. 201 (2006) 1922–1929.
[31] J. Oberste Berghaus, J.G. Legoux, C. Moreau, F. Tarasi, T. Chraska, J. Therm. Spray Technol. 17 (1) (2008) 91–104.
[32] S. Sodeoka, M. Suzuki, K. Ueno, H. Sakuramoto, R. Shibata, M. Ando, Thermal and mechanical properties of ZrO_2–CeO_2 plasma-sprayed coatings, J. Thermal Spray Technol. 6 (3) (1997) 361–367.
[33] X. Zhang, M. Robertson, C. Decés-Petit, Y. Xie, R. Hui, S. Yick, E. Styles, J. Roller, O. Kessler, R. Maric, D. Ghosh, J. Power Sources 161 (2006) 301–307.
[34] H.L. Tuller, A.S. Nowick, J. Electrochem. Soc. 122 (1975) 255–259.
[35] T. Kudo, H. Obayashi, J. Electrochem. Soc. 123 (1976) 415–419.
[36] M. Gödickemeier, L.J. Gauckler, J. Electrochem. Soc. 145 (1998) 414–421.

[37] T. Matsui, T. Kosaka, M. Inaba, A. Mineshige, Z. Ogumi, Solid State Ionics 176 (7–8) (2005) 663–668.
[38] T. Matsui, M. Inaba, A. Mineshige, Z. Ogumi, Solid State Ionics 176 (2005) 647–654.
[39] A. Atkinson, Solid State Ionics 95 (3–4) (1997) 249–258.
[40] X. Zhang, M. Robertson, C. Decès-Petit, Y. Xie, R. Hui, W. Qu, O. Kesler, R. Maric, D. Ghosh, J. Power Sources 175 (2008) 800–805.
[41] Z. Bi, B. Yi, Z. Wang, Y. Dong, H. Wu, Y. She, M. Cheng, Electrochem. Solid-state Lett. 7 (5) (2004) A105–A107.
[42] J. Park, E.D. Wachsman, Ionics 12 (2006) 15–20.
[43] S. Taniguchi, M. Kadowaki, H. Kawamura, T. Yasuo, Y. Akiyama, Y. Miyake, T. Saitoh, J. Power Sources 55 (1995) 73–79.
[44] S.P.S. Badwal, R. Deller, K. Foger, Y. Ramprakash, J.P. Zhang, Solid State Ionics 99 (1997) 297–310.
[45] S.C. Paulson, V.I. Birss, J. Electrochem. Soc. 151 (2004) A1961–A1968.
[46] S.P. Jiang, S. Zhang, Y.D. Zhen, J. Electrochem. Soc. 153 (2006) A127–A134.
[47] S.P. Jiang, J.P. Zhang, K. Foger, J. Electrochem. Soc. 147 (2000) 3195–3205.